ARTICLE

Solar Cells Based on Block Copolymer Semiconductor Nanowires: Effects of Nanowire Aspect Ratio

Guoqiang Ren, Pei-Tzu Wu, and Samson A. Jenekhe*

Department of Chemical Engineering and Department of Chemistry, University of Washington, Seattle, Washington 98195, United States

ABSTRACT The solution-phase self-assembly of nanowires (NWs) from diblock copolymer semiconductors, poly(3-butylthiophene)-*block*-poly(3-octylthiophene), of different block compositions gave crystalline NWs of similar width (13−16 nm) but a tunable average aspect ratio (length/width) of 50−260. The power conversion efficiency of bulk heterojunction solar cells comprising the diblock copolythiophene NWs and $PC_{71}BM$ was found to increase with increasing aspect ratio, reaching 3.4% at the highest average aspect ratio of 260. The space charge limited current mobility of holes in neat films of the copolymer NWs and in copolymer NWs/$PC_{71}BM$ films (~1.0×10^{-4} $cm^2/(V\ s)$) was invariant with aspect ratio, reflecting the parallel orientation of the NWs to the substrate. The enhancement of photovoltaic efficiency with increasing aspect ratio of NWs was explained in terms of increased exciton and charge photogeneration and collection in the bulk heterojunction solar cells.

KEYWORDS: block copoly(3-alkylthiophene) nanowire · nanowire aspect ratio · polymer solar cell · charge transport · block copolymer semiconductor · photovoltaic properties · solution-phase self-assembly

Solar cells made from organic/polymer semiconductors are promising low cost alternative to conventional photovoltaic devices based on inorganic semiconductors.[1−4] However, because photogenerated excitons in polymer solar cells have relatively small diffusion lengths (5−20 nm)[1−3,5,6] and a large binding energy (*ca.* 0.4−1.0 eV),[3−5] the multicomponent organic/polymer active layer in bulk heterojunction (BHJ) cells[7] must necessarily be structured on the same scale as the exciton diffusion length to be highly efficient.[1−5,8,9] Among the new approaches to realizing the two-phase nanostructured morphology in such polymer/fullerene BHJ solar cells are the use of a processing additive during the spin coating of the BHJ thin film,[10,11] the use of self-assembled polymer semiconductor nanowires (NWs),[12−17] and the use of the microphase separation of a diblock copolymer containing one or both conjugated polymer blocks.[18−27] Block copolymers containing one or more π-conjugated polymer blocks are of increasing interest as an approach to the two-phase BHJ thin film morphology with nanoscale domain sizes for application in solar cells.[19−22,28]

In the case of NWs of conjugated homopolymers, the primary focus has been on regioregular poly(3-alkylthiophene)s and especially poly(3-hexylthiophene) (P3HT),[16,29−34] poly(3-pentylthiophene) (P3PT),[15,30] and poly(3-butylthiophene) (P3BT).[12−14,30,31,35] Highly crystalline NWs of *ca.* 8−30 nm widths, 3−5 nm thickness, and lengths of up to 1−10 μm have been assembled from solutions of P3BT,[12−14] P3PT,[15] and P3HT[16] and exploited in the construction of efficient BHJ solar cells. Although the width and thickness of self-assembled NWs of poly(3-alkylthiophene)s fall in the range comparable to the exciton diffusion length, their lengths and thus aspect ratios are difficult to control,[13] precluding a full understanding of the effects of the nanowire morphology on charge transport and photovoltaic properties of polymer semiconductor NWs. Indeed, we know of no literature report on any method to control the length or aspect ratio of solution-phase assembled conjugated polymer NWs nor of a study of effects of the aspect ratio on their properties and device applications.

In this paper, we report the solution-phase self-assembly, morphology, charge transport, and photovoltaic properties of diblock copoly(3-alkylthiophene) NWs. We show that the copolymer composition provides a means to tune the aspect ratio (length/width, *L*/*d*) of NWs assembled from the block copolythiophenes. The vertical charge transport through the copolymer NWs/fullerene BHJ thin films was characterized by space charge limited current measurement and found to be independent of aspect ratio of the NWs. In contrast, the

*Address correspondence to jenekhe@u.washington.edu.

Received for review July 26, 2010 and accepted December 1, 2010.

Published online December 7, 2010. 10.1021/nn1017632

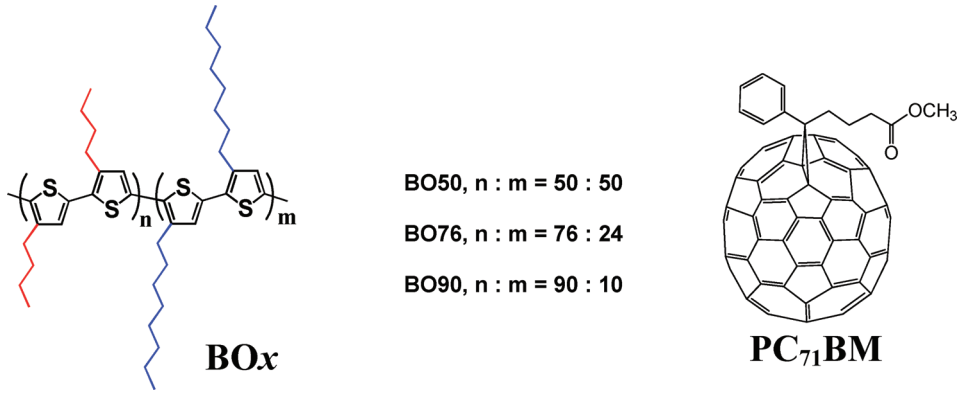

Scheme 1. Structures of the diblock copoly(3-alkylthiophene)s, BO*x*, and $PC_{71}BM$.

power conversion efficiency of the copolymer NWs/fullerene BHJ solar cells varied with the aspect ratio of the NWs. The molecular structures of the diblock copoly(3-alkylthiophene)s investigated in this study, poly(3-butylthiophene)-*block*-poly(3-octylthiophene) (BO*x*, where *x* refers to the percent molar fraction of P3BT segment in the diblock copolymers), and [6,6]-phenyl-C_{71} butyric acid methyl ester ($PC_{71}BM$) are shown in Scheme 1.

RESULTS AND DISCUSSION

Assembly and Morphology of Block Copolythiophene NWs.

The solution-phase self-assembly of NWs from the diblock copolythiophenes BO*x* is similar to our previously described methods for the assembly of NWs from poly(3-butylthiophene) homopolymer.[12,14] We note that although five different block compositions of BO*x* (x = 17, 29, 50, 76, and 90) were synthesized and previously studied,[19,21] here we focused on BO50, BO76, and BO90 nanowire growth by solution-phase self-assembly in *ortho*-dichlorobenzene (ODCB). Under similar conditions, NWs could not be assembled from BO17 and BO29. By maintaining the concentration of each BO*x* (BO50, BO76, and BO90) in ODCB at 10 mg/mL (1 wt %) while varying the temperature from room temperature (20 °C) to 80 °C, we were able to tune the morphology of the NWs. Figure 1 shows the morphology of the diblock copolythiophene NWs revealed by TEM and AFM images. The TEM images show that NWs obtained from the three diblock copolymers, BO50, BO76, and BO90, had widths of 13.3 ± 1.1, 15.8 ± 1.5, and 14.5 ± 1.0 nm, respectively, based on 100 measurements of the width and length of NWs in TEM images. Although the width (d) of the NWs (13−16 nm) is relatively narrow in distribution across the different block compositions, the length (L) distribution and thus aspect ratio (L/d) was quite broad. The aspect ratio varied from 15 to 75 in BO50[19] and 25−115 in BO76 to 125−350 in BO90. The average aspect ratio of these diblock copolythiophene NWs were 48 ± 13, 80 ± 27, and 263 ± 46 for the BO50, BO76, and BO90 NWs, respectively. The observed morphology of BO50 NWs corresponds well with our previous report.[19] However, the NWs of BO76 and BO90, investigated here for the

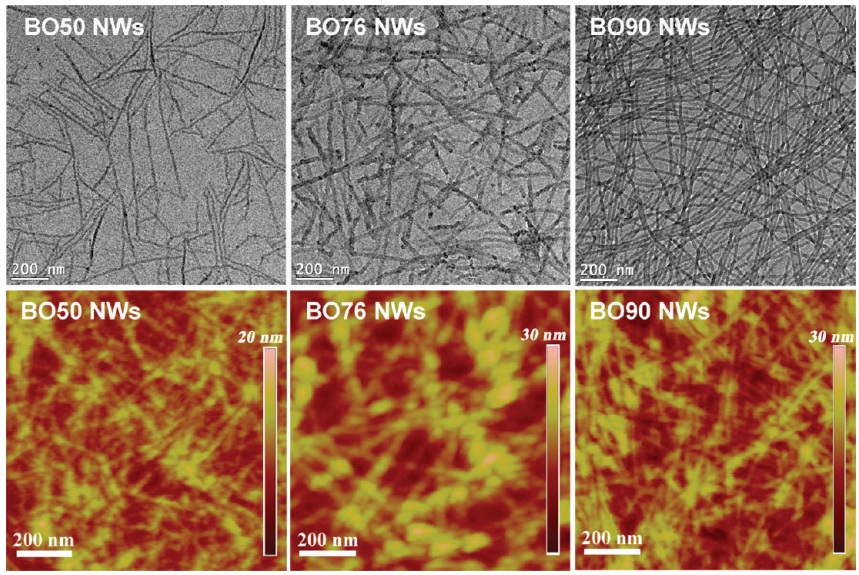

Figure 1. BF-TEM and AFM topographical images of NWs assembled from diblock copolythiophenes of different compositions: BO50, BO76, and BO90.

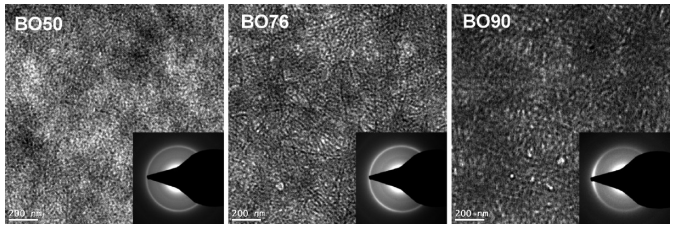

Figure 2. TEM images of pure block copolymer nanowire films.

first time, have significantly higher aspect ratios compared to BO50. Since the BO*x* samples have comparable molecular weights, the huge difference in aspect ratio is attributable to the variation in block composition and perhaps also the dissolution temperature. On the other hand, we note that when BO50 solution was heated above 50 °C, assembly of NWs became difficult and only spherical aggregates of BO50 then result, suggesting that temperature is not a significant factor controlling the aspect ratio of BO*x* NWs. The AFM images (Figure 1) confirmed the morphology of NWs observed in TEM images.

Figure 2 shows the TEM images of spin-coated thin films of the BO*x* NWs. It is obvious that the nanofiber morphology is maintained in the films, and even without any thermal annealing, these NWs show high crystallinity as indicated by the selected area electron diffraction (SAED) patterns shown in the inset of Figure 2. The fact that in SAED, diffraction signals are only collected from a small angle[36] up to 3−5° makes the detection of reflections from π−π stacking in polymers possible.[37,38] The bright outer rings in all the SAED patterns corresponds to (020) diffraction peak in the *q*-vector range of 2.5−2.6 nm^{-1}, indicating that the π-stacking distance in films of BO*x* NWs is 0.38−0.40 nm. This π-stacking distance in films of diblock copolythiophene NWs is comparable to that in films of poly(3-alkylthiophene) homopolymers.[29] The observed SAED rings for BO50 and BO76 NWs are isotropic, indicating that these NWs arrange themselves randomly since there is no control over the orientation of the NWs. However, the SAED pattern for BO90 NWs appears to be anisotropic, which may be a result of oriented NWs in the small area sampled.

The crystallinity and molecular packing in the diblock copolythiophene NWs were further confirmed by the X-ray diffraction (XRD) spectra shown in Figure 3a. The NWs of BO50, BO76, and BO90 show diffraction peaks that are characteristic of P3OT and P3BT blocks. In BO50 NWs, the observed interchain spacing (d_{100}) of 2.00 nm corresponds to that in P3OT block, while a shoulder that appears at a $2\theta = 6.10°$ is characteristic of P3BT block (d_{100} = 1.45 nm).[39] In NWs of BO76 and BO90, a prominent peak corresponding to the P3BT block was observed with a d_{100} spacing of 1.36 and 1.38 nm, respectively. A shoulder at $2\theta = 5.19°$ is visible in the XRD spectrum of BO76 NWs, corresponding to a *d*-spacing of 1.70 nm. It is obvious that in the assembly of the BO*x* NWs, the constituent P3OT and P3BT blocks organize in such a way that the lamellar spacings (d_{P3OT} and d_{P3BT}) are modified compared with the parent homopolymers (P3OT, P3BT). Combining information from both SAED and XRD, the molecular packing in these diblock copolythiophene NWs is proposed and schematically illustrated[19] in Figure 3b. The axis of the NWs is extended along the (010) or the π-stacking direction. In the (100) direction, the NWs are stacked by side-chain organization.

Bulk Heterojunction Solar Cells. The width of these copolythiophene NWs (13−16 nm) is comparable to the exciton diffusion length in polymer semiconductors (5−20 nm)[1−3,5,6] and thus falls into the optimum distance for exciton dissociation in polymer solar cells. The crystalline nature of the copolymer NWs and their varying aspect ratios also suggest the possibility of tuning the charge transport and nanoscale morphology of BHJ solar cells.[12,14] We have thus explored BHJ solar cells based on these diblock copolythiophene NWs.

The photovoltaic properties of BO*x* NWs in BHJ solar cells were studied by blending the NWs with an electron acceptor, [6,6]-phenyl-C_{71} butyric acid methyl ester ($PC_{71}BM$), using the device structure: ITO/PEDOT:PSS/active layer/LiF/Al, where the active layer is a BO*x* NWs:$PC_{71}BM$ nanocomposite. The solar cells were characterized under AM1.5 solar illumination at 1 sun (100 mW/cm^2) in laboratory air. Typical current density (*J*)−voltage (*V*) curves for BO50 NWs:$PC_{71}BM$, BO76

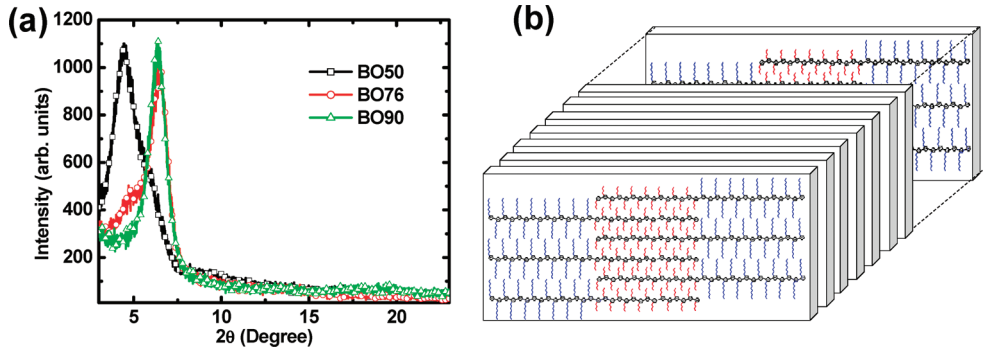

Figure 3. (a) X-ray diffraction spectra of films of BO50, BO76, and BO90 NWs. (b) Schematic illustration of molecular packing in a single BO*x* nanowire.

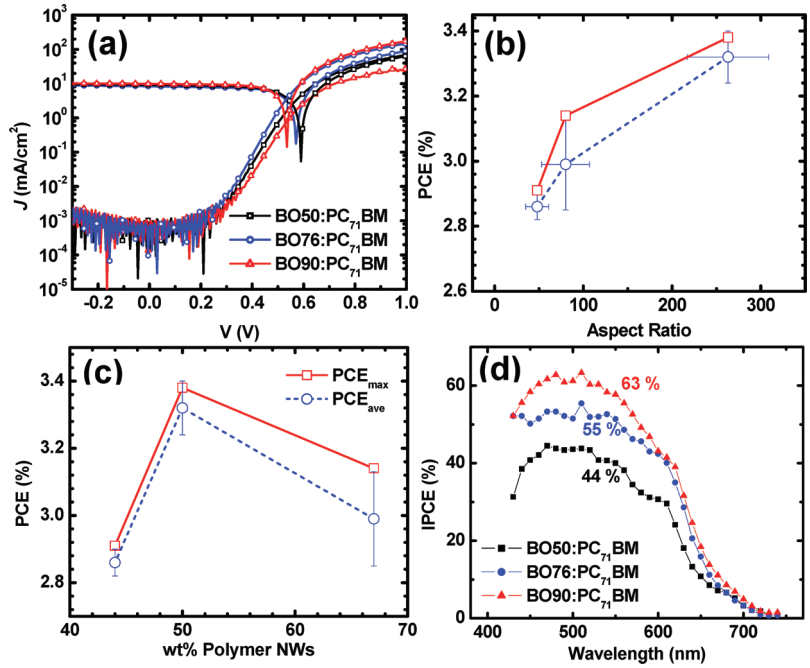

Figure 4. (a) Semilogarithmic plot of the dark current density (*J*)−voltage (*V*) curves and the photocurrent density−voltage curves of solar cells made from BO*x* NWs:$PC_{71}BM$. (b) Plot of maximum (□) and average (○) PCEs *vs* average aspect ratio of NWs. (c) Plot of maximum (□) and average (○) PCEs as a function of BO*x* NWs:$PC_{71}BM$ composition. (d) IPCE of BO*x* NWs:$PC_{71}BM$ solar cells at optimal blend ratios and processing conditions. BO50 NWs:$PC_{71}BM$ (1:1.25), BO76 NWs:$PC_{71}BM$ (1:0.5), and BO90 NWs:$PC_{71}BM$ (1:1) thin films were processed by 30 min, 120 min, 90 min film aging, respectively, followed by 5 min thermal annealing at 110 °C.

NWs:$PC_{71}BM$, and BO90 NWs:$PC_{71}BM$ thin film solar cells are shown in Figure 4a. The photovoltaic parameters calculated from the *J*−*V* curves are summarized in Table 1. The observed open circuit voltage (V_{oc}) was 0.53−0.59 V, which is comparable to BHJ solar cells from the homopolymers, P3BT and P3OT.[21] The short-current density (J_{sc}) increased from 8.31 mA/cm² in BO50 NWs to 9.85 mA/cm² in devices based on BO90 NWs. The fill factor of 0.58−0.65 is comparable to, and even higher than, values found in P3BT NWs:$PC_{61}BM$ devices.[12,14] These photovoltaic parameters translate to a maximum power conversion efficiency (PCE) of 2.91, 3.14, and 3.38%, and an average PCE of 2.86, 2.99, and 3.32% for BO50 NWs, BO76 NWs, and BO90 NWs BHJ devices, respectively. We note that the larger standard deviation in the average PCE of BO76 NWs:$PC_{71}BM$ solar cells may be due to the higher polymer content in this composite, which could have slowed the drying of the film and caused local heterogeneity. We also note that the small difference in PCEs between BO50 NWs:$PC_{71}BM$ and BO76 NWs:$PC_{71}BM$ solar cells arise from the small difference in their aspect ratios (48 ± 13 *vs* 80 ± 27). Compared with the best BHJ devices based on P3BT NWs:$PC_{71}BM$ (3.0−3.2% PCE),[12] the BO*x* NW devices have a comparable efficiency, and in the case of 3.4% PCE obtained for BO90 NWs, is even slightly higher.

The maximum and average efficiencies of BO*x* NW solar cells are plotted as a function of the average aspect ratio (*L*/*d*) of NWs, as shown in Figure 4b. A significant increase of both maximum and average PCEs with aspect ratio is observed, demonstrating that nanowires with high aspect ratio are beneficial in BHJ polymer solar cells. In contrast, the dependence of average and maximum efficiencies on the BO*x* NWs:$PC_{71}BM$ composition is nonmonotonic as shown in Figure 4c. The incident photon-to-electron efficiency (IPCE) or action spectrum of each BO*x* NW solar cell is shown in Figure 4d. The photoresponse of these BHJ diodes turns on at about 730 nm and peaks at ~510 nm. Compared with solar cells based on blend thin films of the same block copolymers,[21] the IPCE maxima in the nanowire devices are red-shifted by 20 nm, an indication that more photons in the solar spectrum can be harvested

TABLE 1. Charge Transport and Photovoltaic Properties of BO*x* NWs:$PC_{71}BM$ Solar Cells

blends	processing condition[a]	μ_h[b] (cm^2/V s)	r_s (Ω cm^2)	r_p (Ω cm^2)	J_{sc} (mA/cm^2)	V_{oc} (V)	FF	PCE_{max} (%)	PCE_{ave}[c] (%)
BO50:$PC_{71}BM$ (1:1.25)	30 min FA, 5 min TA	2.22×10^{-4}	10.3	449	8.31	0.57	0.62	2.91	2.86 ± 0.04
BO76:$PC_{71}BM$ (1:0.5)	120 min FA, 5 min TA	7.03×10^{-5}	12.2	867	9.20	0.59	0.58	3.14	2.99 ± 0.14[d]
BO90:$PC_{71}BM$ (1:1)	90 min FA, 5 min TA	1.72×10^{-4}	7.5	903	9.85	0.53	0.65	3.38	3.32 ± 0.08

[a]FA: film aging, TA: thermal annealing. [b]β values for BOx:$PC_{71}BM$ (x = 50, 76, 90) are -1.70×10^{-4} $(m/V)^{1/2}$, -1.06×10^{-4} $(m/V)^{1/2}$, and -1.84×10^{-4} $(m/V)^{1/2}$, respectively. [c]Average based on 5 devices with standard deviation. [d]Average based on 10 devices with standard deviation.

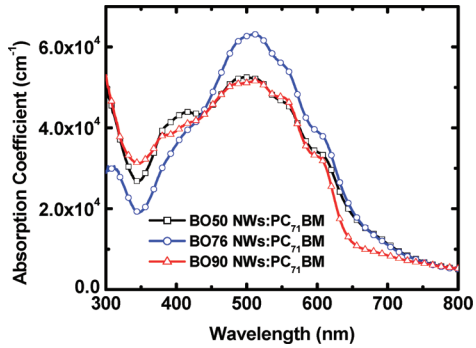

Figure 5. The absorption spectra of BO*x* NWs:$PC_{71}BM$ films measured directly from solar cells.

and transformed to electrical current. The maximum IPCE was 44% for BO50 NWs:$PC_{71}BM$, 55% for BO76 NWs:$PC_{71}BM$, and 63% for BO90 NWs:$PC_{71}BM$ devices. The IPCE thus increases with increasing aspect ratio of the diblock copolymer NWs, similar to the trend of PCE with aspect ratio. We note that the IPCE value of BO90 NWs/$PC_{71}BM$ devices (63%) is close to those reported for P3HT/fullerene BHJ solar cells.[40,41]

The electrical parameters of the copolythiophene NW solar cells were evaluated. The BO*x* NWs-based solar cells had good diode characteristics as indicated by the very high rectification ratios (680−2300 in the dark at ±0.60 V), and the large shunt resistance ($r_p \approx$ 450−900 Ω cm^2) derived from the inverse of the slope at open-circuit conditions. On the other hand, the series resistance (r_s) obtained from the inverse of the slope at short-circuit conditions is in the range of 7.5−12.2 Ω cm^2, which is decreased compared with 13.5−21.1 Ω cm^2 observed in P3BT NWs:$PC_{61}BM$ solar cells.[14] The decreased series resistance of BO*x* NWs:$PC_{71}BM$ thin films (95−105 nm) is attributed to the decreased thickness compared with P3BT NWs:$PC_{61}BM$ thin films (200−230 nm). We also note that the series resistance observed in these BO*x* NWs:$PC_{71}BM$ solar cells is comparable to those of annealed P3HT:$PC_{61}BM$ blends with typical series resistance of 8 Ω cm^2 or less.[42,43]

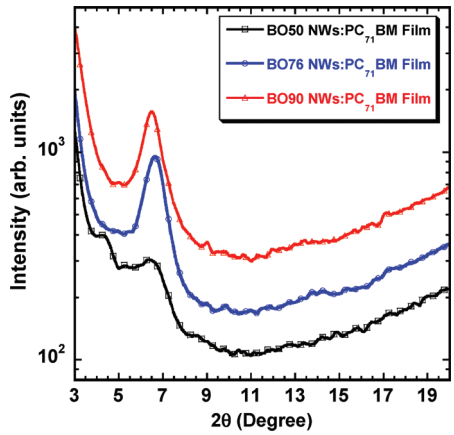

Figure 6. X-ray diffraction of BO*x* NWs:$PC_{71}BM$ thin films on solar cells without cathode deposition.

To gain further insight into the dependence of the performance of BHJ solar cells on nanowire aspect ratio, we investigated the photophysics, charge transport, and morphology of the same BO*x* NWs:$PC_{71}BM$ BHJ films. The thin film absorption spectra of BO50:$PC_{71}BM$ (1:1.25), BO76:$PC_{71}BM$ (1:0.5), and BO90:$PC_{71}BM$ (1:1), which gave the best power conversion efficiency, are shown in Figure 5. The line shape of the spectra, absorption maxima, and absorption coefficient vary with the morphology of the NWs. All the spectra show distinct vibronic shoulders at 560 and 610 nm, indicative of improved interchain π-stacking and crystalline polymer domains in the BHJ thin films. The films of BO50 and BO90 NWs/$PC_{71}BM$ nanocomposites show a similar maximum absorption coefficient of 5×10^4 cm^{-1}, whereas BO76 NWs:$PC_{71}BM$ thin films had a higher value of 6.5×10^4 cm^{-1}. This trend can be explained by the fact that a lower amount of $PC_{71}BM$ is present in the BO76 nanocomposite, which also causes less disruption in the crystalline polymer NW phase. Comparing the absorption spectrum with the IPCE spectrum (Figure 4d) for each BO*x* NWs:$PC_{71}BM$ thin film, the two spectra have similar lineshapes and the same peak position. On the basis of the similar absorption spectra, the higher device efficiency of BO90 NWs:$PC_{71}BM$ solar cells compared to BO50 NWs:$PC_{71}BM$ cannot be fully understood and thus other factors must be considered.

X-ray diffraction (XRD) was used to investigate the morphology and molecular packing in the BO*x* NWs:$PC_{71}BM$ BHJ thin films (80−100 nm). The XRD data were collected directly from the BHJ thin films without the LiF/Al cathode (Figure 6). BO50 NWs:$PC_{71}BM$ film shows two distinct reflections with 2θ angles of 4.39° and 6.29°, corresponding to *d*-spacings of 2.01 and 1.40 nm, respectively. In the case of BO76 and BO90 NWs, only one dominant reflection from the P3BT blocks was detected at 6.67° and 6.43°, with corresponding *d*-spacings of 1.32 and 1.37 nm, respectively. These *d*-spacings indicate that the interchain distances between polymer backbones are in good agreement with the *d*-spacing values for the pure BO50 and BO76 NWs.[19] This means that the molecular packing in the NWs is not significantly affected by $PC_{71}BM$ in the nanocomposites, or the processing conditions (film aging and thermal annealing).

The morphology of BO*x* NWs:$PC_{71}BM$ films peeled directly from the solar cells were investigated by BF-TEM. The images were taken at slightly defocused conditions to enhance the contrast between crystalline and amorphous phases (Figure 7). The polymer phase is presumably the brighter phase and $PC_{71}BM$ is the darker phase due to density difference.[37] NWs are present in the BO*x* NWs:$PC_{71}BM$ films as interconnected networks of the block copolymer donor phases. The darker phase in the images represents the distribution of $PC_{71}BM$ and it can be seen that these $PC_{71}BM$ domains are interconnected with sizes less than 50 nm. SAED was em-

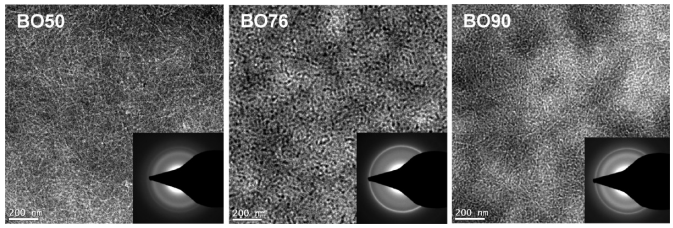

Figure 7. TEM images of BO*x* NWs:$PC_{71}BM$ thin films peeled from solar cells and their SAED patterns (inset).

ployed to probe the changes of crystallinity in the BHJ thin films and the results are shown in the insets of Figure 7. The bright outer rings in the SAED patterns indicate that the π-stacking distances of the diblock copolythiophene NWs in the blend films are 0.38−0.40 nm, which means that the π-stacking in the NWs is not destroyed by the presence of $PC_{71}BM$. The inner rings in the SAED patterns are $PC_{71}BM$ diffractions positioned at around 2.0−2.1 nm^{-1}, as confirmed by the pure $PC_{71}BM$ reflection peak at 2.04 nm^{-1} in Figure 7. The *d*-spacing for the $PC_{71}BM$ is calculated to be 0.49 nm, which is similar to values of another fullerene derivative, $PC_{61}BM$.[37,38]

The charge-carrier mobility of the NWs and the BO*x* NWs:$PC_{71}BM$ nanocomposites were evaluated by the space charge limited current (SCLC) method. The dark-current density (*J*) *versus* voltage (*V*) curves in the hole-only devices are shown in Figure 8. Zero-field mobilities of holes were extracted from the *J*−*V* curves by nonlinear least-squares fit to the modified Mott−Gurney equation.[14,44] The hole mobility in films of the neat BO50, BO76, and BO90 NWs was calculated to be 1.61 × 10^{-4}, 0.87 × 10^{-4}, and 1.26 × 10^{-4} $cm^2/(V\ s)$, respectively. The corresponding β values, which show the electric field dependence of mobility, were −2.10 × 10^{-4} $(m/V)^{1/2}$, −1.89 × 10^{-4} $(m/V)^{1/2}$, and −1.63 × 10^{-4} $(m/V)^{1/2}$, respectively. The SCLC mobilities of holes in the BO*x* NWs:$PC_{71}BM$ nanocomposites, which are collected in Table 1, showed very similar values as the films of the neat NWs. This means that the aspect ratio of the NWs does not influence the SCLC carrier mobility in the vertical direction of the thin films. The observed independence of SCLC carrier mobility as a function of aspect ratio is in line with the fact that the NWs in the BHJ thin films are largely parallel to the substrate. These SCLC hole mobilities are comparable to that of P3HT in annealed P3HT:$PC_{61}BM$ (1:1) blends (2 × 10^{-4} $cm^2/(V\ s)$)[45] and are one- or two-order of magnitude higher than those in P3OT:$PC_{71}BM$ (2.91 × 10^{-5} $cm^2/(V\ s)$) and P3BT:$PC_{71}BM$ (4.26 × 10^{-6} $cm^2/(V\ s)$) blends, respectively.[21] We note that, similar to that of P3BT NWs:$PC_{61}BM$ solar cells, the hole mobility of these BO*x* NWs:$PC_{71}BM$ blends shows a negative electric field dependence.[14] These β values are comparable among BO*x* NWs and BO*x* NWs:$PC_{71}BM$ thin films, regardless of block composition and aspect ratio of NWs. The lack of dependence of SCLC hole mobility on aspect ratio in both neat BO*x* NWs and BO*x* NWs:$PC_{71}BM$ thin films means that the aspect-ratio-dependent photovoltaic properties are not likely to be caused by variations in hole transport.

In summary, we have found that the performance (PCE, IPCE) of BHJ solar cells based on diblock copolythiophene NWs increases with increasing aspect ratio of the nanowires. Although the absorption (and thus light harvesting) and charge carrier (SCLC) mobility of holes are enhanced in these nanowire-based BHJ devices, compared to similar blend or homopolymer devices, these factors could not explain the observed dependence of power conversion efficiency and IPCE on aspect ratio of the block copolymer NWs. In the light of the observed morphology, although the NWs have similar widths within the nanocomposites with $PC_{71}BM$, the variation in the aspect ratio seems to influence performance of the BHJ solar cells in subtle ways. The introduction of donor materials in the form of polymer nanowires also allows a more uniform nanoscale mixing between donors and acceptors in the BHJ thin films. Since long nanowires facilitate the formation of interconnected network and bicontinuous, percolated phase separation, NWs with high aspect ratios would facilitate a higher rate of exciton generation and dissociation, and subsequent charge transport and collection. Additional studies of exciton dissociation and charge recombination rates in polymer nanowire-based BHJ so-

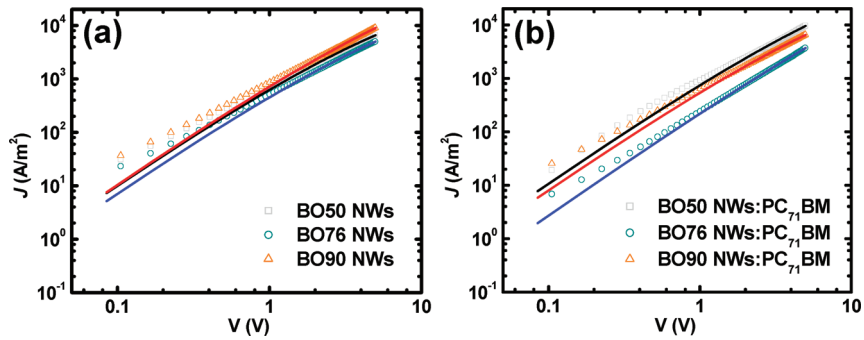

Figure 8. (a) *J*−*V* curves and the corresponding nonlinear least-squares fitting of films of BO*x* NWs (a) and BHJ BO*x* NWs:$PC_{71}BM$ films (b). The thickness of BO*x* NW (*x* = 50, 76, 90) films is 73 nm, 66 nm, and 68 nm, respectively, and 81 nm, 93 nm, and 79 nm for BO*x* NWs:$PC_{71}BM$ films.

lar cells are necessary to fully understand the observed aspect ratio dependence of photovoltaic efficiency.

CONCLUSIONS

We have synthesized NWs with tunable aspect ratio from a series of block copoly(3-alkylthiophene)s through solution phase self-assembly. TEM imaging of the morphology of these NWs showed that the one-dimensional polymer nanostructures had a width of 13−16 nm and average aspect ratio of 48 ± 13, 80 ± 27, and 263 ± 46 for BO50, BO76, and BO90 NWs, respectively. The results show that the diblock copolymer composition provides a facile and powerful means of tuning the aspect ratio of polymer semiconductor nanowires. Bulk heterojunction solar cells based on BO*x* NWs/$PC_{71}BM$ nanocomposites showed a dependence of photovoltaic efficiency (2.9−3.4% PCE) on aspect ratio of the NWs. TEM imaging showed that an interconnected network of polymer NWs with nanoscale donor/acceptor phase separation was achieved. The crystallinity of both copolymer and $PC_{71}BM$ phases was revealed by SAED, as indicated by the intensity of reflection peaks from π-stacking in the copolymer phase and $PC_{71}BM$ crystallites, respectively. The SCLC charge mobility of holes in the BHJ solar cells was invariant with the aspect ratio of the nanowires because of the parallel orientation of the NWs to the substrate. The observed aspect-ratio-dependent photovoltaic properties of the BO*x* NWs are attributed to enhanced charge separation, transport, and collection in the BHJ devices. We conclude that polymer semiconductor NWs with high aspect ratio (length/width > 125−350) are desirable for improving the performance of BHJ solar cells.

EXPERIMENTAL SECTION

Materials and Assembly of Nanowires. The synthesis of the series of block copoly(3-alkylthiophene)s was previously reported.[19] The molecular weight, regioregularity, and thermal properties of BO*x* are summarized in Table 2. The assembly of BO50, BO76, and BO90 NWs was done in *ortho*-dichlorobenzene (ODCB, Sigma-Aldrich, anhydrous, 99%) solution, following our previously reported methods.[12,19] In general, a 10 mg sample (BO*x*) was dissolved in 1 mL of N_2-degassed ODCB and magnetically stirred at a selected temperature until complete dissolution. Because of the difference in solubility, BO50, BO76, and BO90 were prepared at room temperature (20 °C), 50, and 80 °C, respectively. Each of the resulting solution was passed through a 0.45 μm filter, cooled to room temperature, and allowed to grow NWs undisturbed for two days. Thus, a 10 mg/mL (1 wt %) suspension each of BO50, BO76, and BO90 NWs was obtained.

Preparation of BOx Nanowire:Fullerene Nanocomposites. A 60 mg/mL [6,6]-phenyl-C_{71} butyric acid methyl ester ($PC_{71}BM$) solution in ODCB was prepared at room temperature and passed through a 0.45 μm filter. Nanocomposites were prepared by blending a suspension of BO*x* NWs with a $PC_{71}BM$ solution at desired weight ratios and stirred well before spin-coating to fabricate devices.

Device Fabrication and Characterization. Solar cells were fabricated on indium tin oxide (ITO) glass substrates. ITO substrates (10 Ω/□, Shanghai B. Tree Tech. Consult Co., Ltd., Shanghai, China) were cleaned sequentially with acetone, deionized water, and isopropyl alcohol in an ultrasonic bath and blown with nitrogen until they were dried. A 50 nm PEDOT:PSS (Baytron P VP AI 4083) layer was spin-coated on top of the ITO and dried at 150 °C for 10 min under vacuum. Each BO*x* NWs:$PC_{71}BM$ suspension was spin-coated on top of PEDOT:PSS layer for 30 s in a glovebox to make a BHJ active layer. The thickness of each BO*x* NWs:$PC_{71}BM$ (x = 50, 76, 90) thin film was 105, 95, and 100 nm, respectively. The photovoltaic properties of the BO*x* NWs:$PC_{71}BM$ nanocomposites were optimized by first testing several BO*x* NWs:$PC_{71}BM$ ratios (1:0.5, 1:0.75, 1:1, and 1:1.25) followed by further device optimization (thermal annealing, film aging) at the composition that gave the best PCE. Device optimization techniques, such as film aging in a Petri dish and thermal annealing (at (110 ± 10) °C for 5 min), were carried out. The substrates were then loaded in a thermal evaporator (BOC Edwards, 306) to deposit a cathode composed of 1.0 nm LiF and 80 nm Al under high vacuum (8×10^{-7} Torr). Five solar cells, each with an active area of 4 mm^2, were fabricated per ITO substrate. Devices for space-charge limited current (SCLC) measurement were fabricated with the same device structure, except that a Au top electrode was deposited instead of LiF/Al, to facilitate hole-only transport.

Current−voltage characteristics of the solar cells and SCLC devices were obtained using an HP4155A semiconductor parameter analyzer in laboratory ambient air. We note that our solar cell devices were not encapsulated, and thus to minimize the impact of ambient conditions (oxygen, water, *etc.*) on the performance of the solar cells, they were kept in a desiccator before testing in air. One Sun illumination (AM1.5 at 100 mW/cm^2) was provided by a filtered Xe lamp and calibrated by using a calibrated Si diode from the National Renewable Energy Lab (NREL, USA). $J-V$ characteristics for SCLC were measured under dark condition. Zero-field mobilities of holes were extracted from the $J-V$ curves by nonlinear least-squares fit to the modified Mott−Gurney eq:[44]

$$J = \frac{9}{8}\varepsilon\varepsilon_0\mu\frac{V^2}{L^3}\exp\left(\frac{0.89\beta\sqrt{V}}{\sqrt{L}}\right) \quad (1)$$

where J is the current density, V is the applied voltage, L is the active layer thickness, μ is the mobility, ε is the relative permittivity, ε_0 is the permittivity of free space (8.85×10^{-12} F/m), and β is the field-activation factor (also called the electric field coefficient). The solid lines in Figure 8 represent the fitting curves based on this model. The electric field dependent value of charge carrier mobility can be calculated accordingly.[46,47]

Measurement of the incident photon to current efficiency (IPCE) was made using an Oriel xenon lamp (450 W) with an Oriel Cornerstone 130 1/8 m monochromator. The signal was measured with a calibrated standard silicon solar cell and KG5 filter which was calibrated at NREL using a SR830 DSP lock-in amplifier at a chopping frequency of 400 Hz.

Characterization of Morphology and Absorption Spectra. X-ray diffraction (XRD) of the neat BO*x* NWs was done on films drop-casted onto clean silicon wafer and dried in vacuum. A Bruker F8 Focus powder X-ray diffractometer with Cu Kα beam (40 kV, 40 mA; λ = 0.15418 nm) was employed to obtain the XRD spectra. XRD spectra of the BHJ BO*x* NWs:$PC_{71}BM$ blends were acquired on the actual solar cells, whose photovoltaic properties are reported. Imaging by atomic force microscopy (AFM) was done within an area of 5 × 5 μm^2 with a Dimension 3100 SPM (Veeco) instrument operating in tapping mode. For transmission electron microscopy (TEM) imaging, each nanowire suspension was di-

TABLE 2. Molecular Weight, Regioregularity, and Thermal Properties of BO*x*

copolymer	M_w (g/mol)	M_n (g/mol)	PDI	rr (%)	T_m (°C)	T_c (°C)
BO50	29300	17300	1.69	94.1	190, 246	149, 204
BO76	18200	11400	1.60	93.7	263	223
BO90	44900	15800	2.84	94.1	278	234

luted with ODCB, drop-casted onto a TEM grid (300 mesh, carbon-coated copper grids, Electron Microscopy Sciences, Inc.), dried, and examined under bright-field TEM (BF-TEM). In the case of the nanocomposites, a thin film of the BO*x* NWs:$PC_{71}BM$ active layer was first scratched and soaked in deionized water. The active layer was then peeled off the substrate, supported on a TEM grid, and dried for imaging. An FEI Tecnai G^2 F20 TEM operated at 200 kV was employed for BF-TEM imaging. Selected area electron diffraction (SAED) was done on the same TEM, with a 0.031 mm^2 aperture. Images were acquired with a CCD camera and recorded with Gatan DigitalMicrograph software.

UV−vis absorption spectra were recorded with a Perkin-Elmer model Lambda 900 UV/vis/near-IR spectrophotometer on BO*x* NWs:$PC_{71}BM$ thin films spin-coated on top of PEDOT:PSS/ITO substrates, following the same processing conditions for the solar cells. The film thickness was determined by using an Alpha-Step 500 profilometer (KLA-Tencor).

Acknowledgment. Our report is based on research (excitonic solar cells) supported by the U.S. DOE, Basic Energy Sciences, Division of Materials Science, under Award No. DE-FG02-07ER46467. We also acknowledge the NSF (DMR-0805259 and DMR-0120967) for support of the synthesis of polymer semiconductors and the ONR (N00014-1-1148) for studies of nanowire-based bulk heterojunction devices. G. Ren received a fellowship from the Center for Nanotechnology. Part of this work was conducted at the UW NanoTech User Facility, a member of the NSF National Nanotechnology Infrastructure Network (NNIN).

REFERENCES AND NOTES

1. Gunes, S.; Neugebauer, H.; Sariciftci, N. S. Conjugated Polymer-Based Organic Solar Cells. *Chem. Rev.* **2007**, *107*, 1324–1338.
2. Coakley, K. M.; McGehee, M. D. Conjugated Polymer Photovoltaic Cells. *Chem. Mater.* **2004**, *16*, 4533–4542.
3. Thompson, B. C.; Frechet, J. M. J. Polymer−Fullerene Composite Solar Cells. *Angew. Chem., Int. Ed.* **2008**, *47*, 58–77.
4. Dennler, G.; Scharber, M. C.; Brabec, C. J. Polymer−Fullerene Bulk-Heterojunction Solar Cells. *Adv. Mater.* **2009**, *21*, 1323–1338.
5. Blom, P. W. M.; Mihailetchi, V. D.; Koster, L. J. A.; Markov, D. E. Device Physics of Polymer:Fullerene Bulk Heterojunction Solar Cells. *Adv. Mater.* **2007**, *19*, 1551–1566.
6. Alam, M. M.; Jenekhe, S. A. Nanolayered Heterojunctions of Donor and Acceptor Conjugated Polymers of Interest in Light Emitting and Photovoltaic Devices: Photoinduced Electron Transfer at Polythiophene/Polyquinoline Interfaces. *J. Phys. Chem. B* **2001**, *105*, 2479–2482.
7. Yu, G.; Gao, J.; Hummelen, J. C.; Wudl, F.; Heeger, A. J. Polymer Photovoltaic Cells: Enhanced Efficiencies *via* a Network of Internal Donor−Acceptor Heterojunctions. *Science* **1995**, *270*, 1789–1792.
8. Liang, Y.; Wu, Y.; Feng, D.; Tsai, S.-T.; Son, H.-J.; Li, G.; Yu, L. Development of New Semiconducting Polymers for High Performance Solar Cells. *J. Am. Chem. Soc.* **2009**, *131*, 56–57.
9. Liang, Y.; Xu, Z.; Xia, J.; Tsai, S.-T.; Wu, Y.; Li, G.; Ray, C.; Yu, L. For the Bright Future—Bulk Heterojunction Polymer Solar Cells with Power Conversion Efficiency of 7.4%. *Adv. Mater.* **2010**, *22*, E135−E138.
10. Lee, J. K.; Ma, W. L.; Brabec, C. J.; Yuen, J.; Moon, J. S.; Kim, J. Y.; Lee, K.; Bazan, G. C.; Heeger, A. J. Processing Additives for Improved Efficiency from Bulk Heterojunction Solar Cells. *J. Am. Chem. Soc.* **2008**, *130*, 3619–3623.
11. Peet, J.; Kim, J. Y.; Coates, N. E.; Ma, W. L.; Moses, D.; Heeger, A. J.; Bazan, G. C. Efficiency Enhancement in Low-Bandgap Polymer Solar Cells by Processing with Alkane Dithiols. *Nat. Mater.* **2007**, *6*, 497–500.
12. Xin, H.; Kim, F. S.; Jenekhe, S. A. Highly Efficient Solar Cells Based on Poly(3-butylthiophene) Nanowires. *J. Am. Chem. Soc.* **2008**, *130*, 5424–5425.
13. Xin, H.; Reid, O. G.; Ren, G.; Kim, F. S.; Ginger, D. S.; Jenekhe, S. A. Polymer Nanowire/Fullerene Bulk Heterojunction Solar Cells: How Nanostructure Determines Photovoltaic Properties. *ACS Nano* **2010**, *4*, 1861–1872.
14. Xin, H.; Ren, G.; Kim, F. S.; Jenekhe, S. A. Bulk Heterojunction Solar Cells from Poly(3-butylthiophene)/Fullerene Blends: *In Situ* Self-Assembly of Nanowires, Morphology, Charge Transport, and Photovoltaic Properties. *Chem. Mater.* **2008**, *20*, 6199–6207.
15. Wu, P.-T.; Xin, H.; Kim, F. S.; Ren, G.; Jenekhe, S. A. Regioregular Poly(3-pentylthiophene): Synthesis, Self-Assembly of Nanowires, High-Mobility Field-Effect Transistors, and Efficient Photovoltaic Cells. *Macromolecules* **2009**, *42*, 8817–8826.
16. Berson, S.; Bettignies, R. D.; Bailly, S.; Guillerez, S. Poly(3-hexylthiophene) Fibers for Photovoltaic Applications. *Adv. Funct. Mater.* **2007**, *17*, 1377–1384.
17. Kim, F. S.; Ren, G.; Jenekhe, S. A. One-Dimensional Nanostructures of π-Conjugated Molecular Systems: Assembly, Properties, and Applications from Photovoltaics, Sensors, and Nanophotonics to Nanoelectronics. *Chem. Mater.*, published online December 1, 2010, http://pubs.acs.org/doi/full/10.1021/cm102772x.
18. Botiz, I.; Darling, S. B. Optoelectronics Using Block Copolymers. *Mater. Today* **2010**, *13*, 42–51.
19. Wu, P.-T.; Ren, G.; Li, C.; Mezzenga, R.; Jenekhe, S. A. Crystalline Diblock Conjugated Copolymers: Synthesis, Self-Assembly, and Microphase Separation of Poly(3-butylthiophene)-*b*-poly(3-octylthiophene). *Macromolecules* **2009**, *42*, 2317–2320.
20. Wu, P.-T.; Ren, G.; Kim, F. S.; Li, C.; Mezzenga, R.; Jenekhe, S. A. Poly(3-hexylthiophene)-*b*-poly(3-cyclohexylthiophene): Synthesis, Microphase Separation, Thin Film Transistors, and Photovoltaic Applications. *J. Polym. Sci. A* **2010**, *48*, 614–626.
21. Ren, G.; Wu, P.-T.; Jenekhe, S. A. Enhanced Performance of Bulk Heterojunction Solar Cells Using Block Copoly(3-alkylthiophene)s. *Chem. Mater.* **2010**, *22*, 2020–2026.
22. He, M.; Zhao, L.; Wang, J.; Han, W.; Yang, Y.; Qiu, F.; Lin, Z. Self-Assembly of All-Conjugated Poly(3-alkylthiophene) Diblock Copolymer Nanostructures from Mixed Selective Solvents. *ACS Nano* **2010**, *4*, 3241–3247.
23. Botiz, I.; Darling, S. B. Self-Assembly of Poly(3-hexylthiophene)-*block*-polylactide Block Copolymer and Subsequent Incorporation of Electron Acceptor Material. *Macromolecules* **2009**, *42*, 8211–8217.
24. Segalman, R. A.; McCulloch, B.; Kirmayer, S.; Urban, J. J. Block Copolymers for Organic Optoelectronics. *Macromolecules* **2009**, *42*, 9205–9216.
25. Lindner, S. M.; Huttner, S.; Chiche, A.; Thelakkat, M.; Krausch, G. Charge Separation at Self-Assembled Nanostructured Bulk Interface in Block Copolymers. *Angew. Chem., Int. Ed.* **2006**, *45*, 3364–3368.
26. Sommer, M.; Huttner, S.; Wunder, S.; Thelakkat, M. Electron-Conducting Block Copolymers: Morphological, Optical, and Electronic Properties. *Adv. Mater.* **2008**, *20*, 2523–2527.
27. Zhang, Q.; Cirpan, A.; Russell, T. P.; Emrick, T. Donor−Acceptor Poly(thiophene-*block*-perylene diimide) Copolymers: Synthesis and Solar Cell Fabrication. *Macromolecules* **2009**, *42*, 1079–1082.
28. Darling, S. B. Block Copolymers for Photovoltaics. *Energy Environ. Sci.* **2009**, *2*, 1266–1273.
29. Ihn, K. J.; Moulton, J.; Smith, P. Whiskers of Poly(3-alkylthiophene)s. *J. Polym. Sci., Part B* **1993**, *31*, 735–742.
30. Oosterbaan, W. D.; Vrindts, V.; Berson, S.; Guillerez, S.; Douhéret, O.; Ruttens, B.; D'Haen, J.; Adriaensens, P.; Manca, J.; Lutsen, L.; Vanderzande, D. Efficient Formation, Isolation, and Characterization of Poly(3-alkylthiophene) Nanofibres: Probing Order as a Function of Side-Chain Length. *J. Mater. Chem.* **2009**, *19*, 5424–5435.

31. Samitsu, S.; Shimomura, T.; Heike, S.; Hashizume, T.; Ito, K. Effective Production of Poly(3-alkylthiophene) Nanofibers by Means of Whisker Method Using Anisole Solvent: Structural, Optical, and Electrical Properties. *Macromolecules* **2008**, *41*, 8000–8010.
32. Merlo, J. A.; Frisbie, C. D. Field Effect Transport and Trapping in Regioregular Polythiophene Nanofibers. *J. Phys. Chem. B* **2004**, *108*, 19169–19179.
33. Samitsu, S.; Shimomura, T.; Ito, K. Nanofiber Preparation by Whisker Method Using Solvent-Soluble Conducting Polymers. *Thin Solid Films* **2008**, *516*, 2478–2486.
34. Liu, J.; Arif, M.; Zou, J.; Khondaker, S. I.; Zhai, L. Controlling Poly(3-hexylthiophene) Crystal Dimension: Nanowhiskers and Nanoribbons. *Macromolecules* **2009**, *42*, 9390–9393.
35. Lu, G.; Li, L.; Yang, X. Morphology and Crystalline Transition of Poly(3-butylthiophene) Associated with Its Polymorphic Modifications. *Macromolecules* **2008**, *41*, 2062–2070.
36. Bendersky, L. A.; Gayle, F. W. Electron Diffraction Using Transmission Electron Microscopy. *J. Res. Natl. Inst. Stand. Technol.* **2001**, *106*, 997–1012.
37. van Bavel, S. S.; Sourty, E.; de With, G.; Loos, J. Three-Dimensional Nanoscale Organization of Bulk Heterojunction Polymer Solar Cells. *Nano Lett.* **2009**, *9*, 507–513.
38. Yang, X.; van Duren, J. K. J.; Rispens, M. T.; Hummelen, J. C.; Janssen, R. A. J.; Michels, M. A. J.; Loos, J. Crystalline Organization of a Methanofullerene as Used for Plastic Solar-Cell Applications. *Adv. Mater.* **2004**, *16*, 802–806.
39. Wu, P.-T.; Ren, G.; Jenekhe, S. A. Crystalline Random Conjugated Copolymers with Multiple Side Chains: Tunable Intermolecular Interactions and Enhanced Charge Transport and Photovoltaic Properties. *Macromolecules* **2010**, *43*, 3306–3313.
40. Li, G.; Yao, Y.; Yang, H.; Shrotriya, V.; Yang, G.; Yang, Y. "Solvent Annealing" Effect in Polymer Solar Cells Based on Poly(3-hexylthiophene) and Methanofullerenes. *Adv. Funct. Mater.* **2007**, *17*, 1636–1644.
41. Padinger, F.; Rittberger, R. S.; Sariciftci, N. S. Effects of Postproduction Treatment on Plastic Solar Cells. *Adv. Funct. Mater.* **2003**, *13*, 85–88.
42. Ma, W.; Yang, C.; Gang, X.; Lee, K.; Heeger, A. J. Thermally Stable, Efficient Polymer Solar Cells with Nanoscale Control of the Interpenetrating Network Morphology. *Adv. Funct. Mater.* **2005**, *15*, 1617–1622.
43. Chu, C.-W.; Yang, H.; Hou, W.-J.; Huang, J.; Li, G.; Yang, Y. Control of the Nanoscale Crystallinity and Phase Separation in Polymer Solar Cells. *Appl. Phys. Lett.* **2008**, *92*, 103306.
44. Murgatroyd, P. N. Theory of Space-Charge-Limited Current Enhanced by Frenkel Effect. *J. Phys. D* **1970**, *3*, 151–156.
45. Mihailetchi, V. D.; Xie, H.; de Boer, B.; Koster, L. J. A.; Blom, P. W. M. Charge Transport and Photocurrent Generation in Poly(3-hexylthiophene): Methanofullerene Bulk-Heterojunction Solar Cells. *Adv. Funct. Mater.* **2006**, *16*, 699–708.
46. Blom, P. W. M.; de Jong, M. J. M.; van Munster, M. G. Electric-Field and Temperature Dependence of the Hole Mobility in Poly(*p*-phenylene vinylene). *Phys. Rev. B* **1997**, *55*, R656–R659.
47. Domercq, B.; Yu, J. S.; Kaafarani, B. R.; Kondo, T.; Yoo, S.; Haddock, J. N.; Barlow, S.; Marder, S. R.; Kippelen, B. A Comparative Study of Charge Mobility Measurements in a Diamine and in a Hexaazatrinaphthylene Using Different Techniques. *Mol. Cryst. Liq. Cryst.* **2008**, *481*, 80–93.